Research Square

Preprints are preliminary reports that have not undergone peer review.
They should not be considered conclusive, used to inform clinical practice,
or referenced by the media as validated information.

Valorization of Agar extraction residues from the red algae Gelidium sesquipedale as biosorbents for organic and inorganic pollutants

Lhachmi MOUSSAOUI

lhachmi_moussaoui@um5.ac.ma

Mohammed V University of Rabat: Universite Mohammed V de Rabat

Meriem Bamaarouf

Mohammed V University of Rabat: Universite Mohammed V de Rabat

Latifa Saadi

Cadi Ayyad University: Universite Cadi Ayyad

Rachid Jalal

Cadi Ayyad University: Universite Cadi Ayyad

Mohamed Waqif

Cadi Ayyad University: Universite Cadi Ayyad

Imane Eloutar

Mohammed V University of Rabat: Universite Mohammed V de Rabat

Laila Safaadi

University Hassan II Casablanca: Universite Hassan II Casablanca

Abdeslam Abid

Abdelmalek Essaadi University: Universite Abdelmalek Essaadi

Research Article

Keywords: biomaterials, adsorption, Gelidium sesquipedale, diatom, cation exchange capacity

Posted Date: July 4th, 2025

DOI: https://doi.org/10.21203/rs.3.rs-6198731/v1

License: This work is licensed under a Creative Commons Attribution 4.0 International License.
Read Full License

Version of Record: A version of this preprint was published at Chemical Papers on October 21st, 2026.
See the published version at https://doi.org/10.1007/s11696-026-05795-1.

Valorization of Agar extraction residues from the red algae *Gelidium sesquipedale* as biosorbents for organic and inorganic pollutants

Lhachmi Moussaoui[a, b, c]; Meriem Bamaarouf[a]; Latifa Saadi[b]; Jalal Rachid[c]; Waqif Mohamed[b]; Eloutar Imane[a]; Laila Safaadi[d] and Abdeslam Abid[e]

[a]Energy, Materials and Sustainable Development Team (EMDD), Sale School of Technologie, University of Mohamed V of Rabat, Morocco.

[b]Innovative Materials, Energy and Sustainable Development Laboratory (IMED-Lab), Faculty of Science and Technology of Marrakech, Morocco.

[c]Laboratory of Sustainable Development and Health Research, Faculty of Science and Technology of Marrakech, Morocco.

[d]Process Engineering and Environment Laboratory, Faculty of Science and technology Mohamedia, Hassan II University Casablanca, Mohammedia, Morocco.

[e]Laboratory of Applied and Marine Geoscience, Geotechnics and Geohazards (LR3G), Faculty of sciences, university of Abdelmalek Essaadi, Tetouan 93000, Morocco.

Corresponding author address: DR. BOUSHAB LAMRABTINE SAADA MARRAKECH, MOROCCO

Corresponding author email address: lhachmi_moussaoui@um5.ac.ma

Acknowledgments

The authors are grateful to The Moroccan center of analysis and characterization (CAC), affiliated to Cadi Ayyad University, and The national center of scientific and technical research (CNRST), Morocco, for characterizing the samples used.

Author contributions

Conceptualization, Formal analysis, Investigation, Writing - Original draft, Project administration, Methodology: **[Lhachmi Moussaoui].** Validation, Resources, Writing - Reviewing and editing, Supervision, Methodology: [**Meriem Bamaarouf].** Validation, Resources, Writing - Reviewing and editing, Supervision, Methodology: [**Latifa Saadi].** Resources, Visualization: [**Jalal Rachid**]. Validation, Writing - Reviewing and editing: [**Waqif Mohamed].** Visualization: [**Imane Eloutar].** Validation: **[Laila Safaadi]**. Visualization: [**Abdeslam Abid**].

Abstract

The aim of this research is to study the adsorption capacity of methylene blue and methyl orange by *Gelidium sesquipedale* (GS), *Gelidium sesquipedale* residues (GSR) and an equal mixture of algae residues and diatomaceous earth (GRD). To this end, we have carried out a physico-chemical and structural characterization of the three samples (GS, GSR and GRD). *Gelidium sesquipedale* and its residues are rich in lignin (33.22% and 28.60%, respectively) and cellulose (20.29% and 13.31%, respectively). X-ray fluorescence analysis has showed that the mixture of algae residues and diatomaceous earth is rich in silica (72.23%). The equilibrium adsorption capacity of GSR is comparable to that of GS, both higher than GRD, with rapid retention for methylene blue. Methylene blue adsorption follows the Freundlich model. It is described by the pseudo-second-order kinetic model and is minimally influenced by pH variations. These biomaterials have showed potential for various wastewater treatment applications.

Keywords: biomaterials, adsorption, *Gelidium sesquipedale*, diatom, cation exchange capacity.

1. Introduction

Water is a vital resource and the essence of human socio-economic and industrial development. However, human activities contribute to water pollution; wastewater contains physical, chemical, and biological pollutants that must be treated to protect the environment. A range of treatment techniques has been developed following numerous research projects, for instance, the adsorption of pollutants using biodegradable supports. This approach has proved its effectiveness, demonstrating high efficiency(Kone and al., 2012). Biodegradable substrates used for this purpose include fibers, tree bark, eggshells and algae.

Algae are composed of three types of polysaccharides. These include reserve polysaccharides (starch and laminarin), low-molecular-weight polysaccharides for osmotic regulation and structural polysaccharides(Gaël, 2005; Garon-Lardière, 2004). These form the cell wall, which has an architecture similar to that of terrestrial plants(Garon-Lardière, 2004). It consists of a crystalline microfibril phase embedded in a predominantly amorphous phase; the crystalline phase is composed of cellulose, xylans and mannans. Whereas the amorphous phase of algae is characterized by the abundance of anionic polysaccharides, such as galactan, compared with neutral polysaccharides. The wall also contains up to 10% protein(Garon-Lardière, 2004). Diatoms are also unicellular microalgae measuring 2 to 200 µm(Herzi, 2013). Encased in an ornamental bivalve skeleton of silica and pectin, they are found in aquatic environments, soil and air. They feed by photosynthesis, and are indicators of the health of biotopes thanks to the diatom assemblages they colonize (Herzi, 2013; Straub and al., 2014; Vizinet and al., 1995). Diatomaceous earth or diatomite, a siliceous sedimentary rock composed of fossilized diatom remains, is used in filtration treatment processes(Lavoie and Saulnier-Talbot, 2016).

Morocco's geographical position, with two coastlines stretching over 3,500 km, contributes to the richness and diversity of its marine flora(Bengueddour and al., 2014). Seaweed is an undeniably valuable resource, with over 600 species(Benhissoune, 2002). They represent a potential source of medical products(Bengueddour and al., 2014; 高橋裕一 and 日本水産学会誌, 1987), cosmetics products(Bengueddour and al., 2014), and natural antioxidants for the agri-food and pharmacological industries(Bengueddour and al., 2014; Nagai and Yukimoto, 2003). Algae also offer significant potential for pollution control through adsorption. *Ulva lactuca* has been used for the decontamination of chromium and cadmium(Asnaoui and al., 2017). *Cystoseira sedoides*, a type of brown alga, has shown promising results for the decontamination of water with cadmium and copper.

The red alga *Gelidium sesquipedale* is widespread along the Moroccan coast, with significant populations around El Jadida City. The average biomass density is estimated at 800 $g.m^{-2}$(Givernaud and al., 2005) It is also an important resource for agar production. Characterization of the cell wall of red algae indicates the presence of polysaccharides such as cellulose and xylan, which may provide adsorption capacities. Diatoms, unicellular organisms with silica-rich shells, are fossilized in the form of sedimentary rocks known as diatomaceous earth, with the most significant deposits found in Boudinar and the Melilia Nador basin (northeastern Morocco). The high silica content of diatomaceous earth suggests that these materials have a surface structure with electrically charged sites, which favor the adsorption of micropollutants by ion exchange. This research project, therefore, aims to valorize biomaterials such as algae and by-products from the agar manufacturing industry in wastewater treatment, as part of a circular economy approach.

The aim of this research project is to investigate the potential of three biomaterials as adsorbents: raw *Gelidium sesquipedale* algae, *Gelidium sesquipedale* residue and an equal mixture of *Gelidium sesquipedale* residue and diatomaceous earth. As part of their characterization, we also examined the possibility of using them in nested filters for wastewater treatment. To this end, we have carried out physico-chemical characterization (chemical composition, mineral and organic matter content and moisture content) and structural analysis by Fourier transform infrared spectroscopy, X-ray diffraction, scanning electron microscopy, elemental analysis by X-ray fluorescence and loss of ignition. We have also studied the adsorption kinetics of the three materials using a cationic dye, methylene blue, and an anionic dye, methyl orange.

2. Materials and methods

In order to evaluate these biomaterials, it is necessary to carry out a complete characterization which would enable us to predict their behavior in different applications, particularly in the field of water treatment. In the following, the characterization methods that have been adopted in this study.

2.1. Biological materials

2.1.1. Harvesting area

The red seaweed *Gelidium sesquipedale* is collected by SETEXAM, an Agar-Agar production company based in the Moroccan city of Kenitra. Most of the harvest comes from the El Jadida-Jorf Lasfar maritime zone, located on Morocco's Atlantic coast (Fig (A.1)).

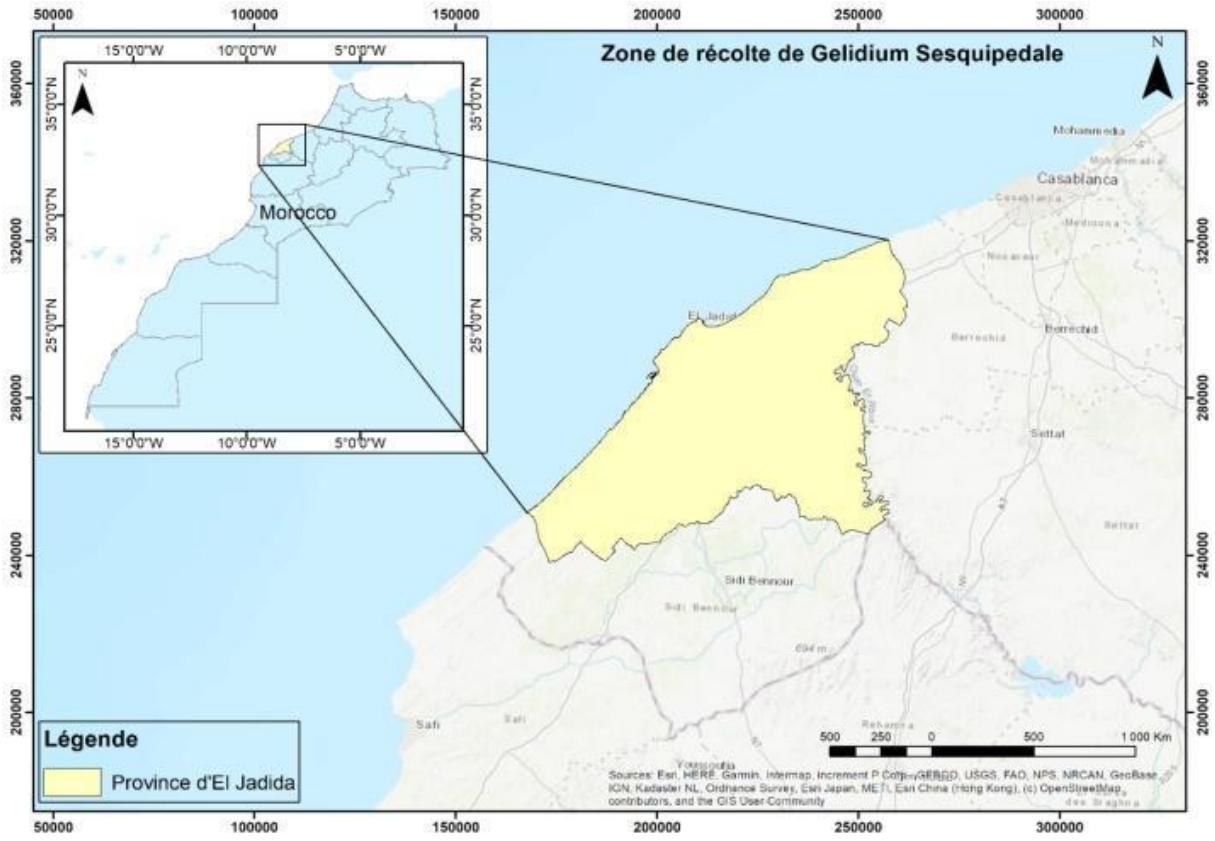


Fig (A.1) The *Gelidium sesquipedale* harvest site

2.1.2. Material composition

The three biomaterials used are illustrated in Fig (A.2) - a) raw *Gelidium sesquipedale* (GS) - b) *Gelidium sesquipedale* residue (GSR) after agar extraction - c) a mixture of 50% diatomaceous earth (used as an adjuvant in the extraction process) and 50% *Gelidium sesquipedale* residue (GRD). These materials were collected at the 'SETEXAM' agar extraction plant in Kenitra. The samples were used in their raw state, without any pre-treatment.



Fig (A.2) adsorbents - a) *Gelidium sesquipedale* (GS) - b) *Gelidium sesquipedale* residue (GSR) - c) The mixture of diatomaceous earth powder and *Gelidium sesquipedale* residue (GRD)

2.1.3. Methylene blue (MB)

Methylene blue (MB) is a dye chosen as a model molecule for medium-sized cationic organic pollutants(Abdallah and al., 2016) (Fig (A.3)).

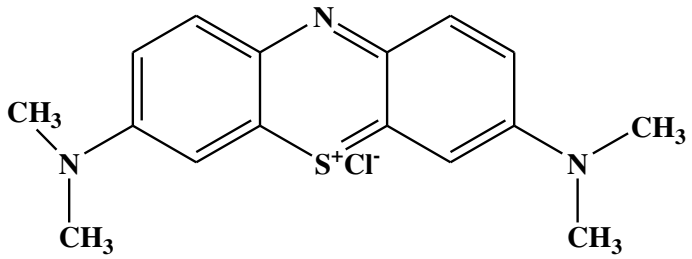


Fig (A.3) Chemical structure of methylene blue (MB)

2.1.4. Methyl orange (MO)

Methyl orange (MO) is a color indicator used in the textile industry, and is also used as a pH indicator for titrations(Elbariji and al., 2006; Iwuozor and al., 2021). This dye was chosen as a model molecule for anionic pollutants (Fig (A.4)).

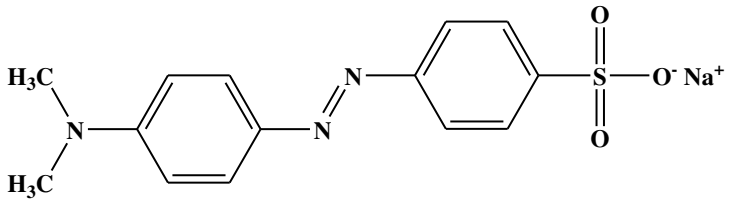


Fig (A.4) Chemical structure of methyl orange (MO)

These two dyes are commonly used as adsorbents to characterize the adsorbency of materials (Abdallah and al., 2016; Elbariji and al., 2006; Iwuozor and al., 2021).

2.2. Physico-chemical characterization

2.2.1. Chemical composition

Cellulose composition: was assessed by the Kurschner and Hoffer method; 2g of the sample was boiled in 100 ml of a mixture of nitric acid and 1/4 (V/V) ethanol for one hour. After filtration, the residue was treated twice using the above procedure. The solid was then washed with distilled water until neutral(Ouensanga, 1989).

Hemicellulose composition: 1 g of sample was immersed in a 5% sodium hydroxide (NaOH) solution at room temperature for 30 minutes, then neutralized with a 10 N hydrochloric acid solution. The sample was then dried in an oven at 105 °C for 2 hours. The difference in weight is recorded as the amount of hemicellulose(Rout and al., 2016).

Lignin composition: was carried out according to the American Society for Testing and Materials (ASTM) procedure: 1g of the sample recovered after treatment with the ethanol-toluene mixture was stirred in 15 ml of 75% sulfuric acid (H_2SO_4) solution for 2 hours. Next, we added 560 ml of water, and the solution is heated to boiling and refluxed for 4 h, to reduce the acid content to 3%. The residue is filtered, washed with 500 ml of water, dried at 105°C and weighed. As lignin is insoluble in 75% sulfuric acid, the residue is essentially lignin(Do Thi, 2011)

Agar composition: 100 g of *Gelidium sesquipedale* is rinsed twice with 1000 ml of water, then soaked in an acid medium for around 30 minutes. After adding 800 ml of water to the recovered sample, the solution was heated to boiling and refluxed for one hour. The extract was then heated for 3 hours and passed through a standard filter. The extract obtained was placed in a container and 100 ml of hot water was added. The agar solution was left to gel at room temperature. The fine-bladed spatula was then used to cut the gel into small squares and the pan was placed in a freezer. The next day, we removed the pan from the freezer and let the gel thaw. Afterwards, the thawed water was drained off and the gel was washed under the tap, rendering it colorless. The agar was finally shredded, placed in a tarred aluminum dish and dried at a temperature of 60°C. Eq (A.1) was used to calculate the mass fraction of Agar-agar(Abraham and al., 2018)

$$\%(\ Agar) = (\frac{W_2}{W_1})*100 \qquad \textbf{(Eq (A.1))}$$

Where W_1 and W_2 are the masses of the algae before and after extraction.

2.2.2. Mineral matter (Mm) and organic matter (Om) content.

We determined mineral content by calcining the samples at 550°C for 4 h, as described in the literature(Ajouguim and al., 2019). The organic matter (Om) content can be deduced using the following expression noted in Eq (A.2).

$$Om\ (\%) = 100 - Mm \qquad \textbf{(Eq (A.2))}$$

Mm is the Mineral matter content and Om is the Organic matter content

2.2.3. Moisture content.

Moisture content was determined in accordance with NF EN ISO 665(Ajouguim and al., 2019; Mouhoubi and al., 2017), and corresponds to the loss in mass after drying at 105 °C to constant mass.

2.2.4. Structural analysis

We carried out structural analysis of the samples by Fourier transform infrared spectroscopy, X-ray diffraction, scanning electron microscopy, elemental analysis by X-ray fluorescence and loss on ignition.

- **Analysis by Fourier Transform Infrared (FTIR) absorption spectroscopy**

It is based on the interactions between infrared radiation and the bonds of the compound in the material to be analyzed. It enables chemical compounds to be identified and molecule structures to be characterized(Dietrich, 2008). Fourier transform infrared (FTIR) spectra were recorded in the range of 400-4000 cm^{-1} using a Bruker Vertex 70 spectrophotometer. Homogeneous pellets containing a mixture of 1 mg algal powder sample with 99 mg KBr were compressed.

- **X-ray diffraction (XRD) analysis**

We used X-ray diffraction (XRD) analysis to identify the phases present in the sample under study(Dietrich, 2008). This analysis was recorded in a 2θ interval ranging from 5 to 70 using a Philips X'Pert MPD diffractometer operating with a copper anode (Kα1 = 1.5418 Â). Thus, the crystallinity index was calculated from the X-ray diffraction data using the Eq (A.3)(Wang and al., 2007). Homogeneous pellets of powdered algal samples deposited on a sample holder.

$$I_{Cr} = \frac{\sum A_{Crystal}}{A_{Total}} *100 \qquad \textbf{(Eq (A.3))}$$

A_{Total} is the sum of the areas under all the diffraction peaks and $\sum A_{Crystal}$ is the sum of the areas corresponding to the crystalline peaks.

- **Scanning electron microscopy (SEM) analysis**

Scanning electron microscopy (SEM) analysis enables microscopic characterization of the sample's contact surface through electron-matter interactions(Dietrich, 2008). It was carried out using a JEOL JSM-5500 (VEGA3 TESCAN) equipped with a Falcon EDAX detector. By taking algal sample fragments glued to a sample holder.

- **X-ray fluorescence (XRF) spectrometry**

We performed X-ray fluorescence (XRF) spectrometry to identify the elemental chemical compounds characterizing the sample under study(Bentahar, 2016). This analysis was carried out using an Axion X-ray fluorescence spectrometer with a 1 kW wavelength dispersion.

- **Loss on ignition (LOI)**

Loss on ignition (LOI) is used to determine the mass of products likely to decompose or volatilize during firing by calcination at 1100°C. After placing the sample in a crucible, it was heated in an oven at a temperature of 1000°C for one hour(Qlihaa and al., 2016). The percentage loss on ignition was calculated as a function of mass difference using Eq (A.4).

$$LOI = \frac{(W_1 - W_2)}{W_1} * 100 \qquad \textbf{(Eq (A.4))}$$

Where W_1 and W_2 are the masses of algae before and after calcination

2.3. Study of BM and OM adsorption

Adsorption experiments were carried out by mixing a 0.25g mass of the material with a 20 mL volume of BM dye solution at C_1=4.12 mg/l, C_2=8.25 mg/l and C_3=16.5 mg/l or OM dye at C_1=1.25 mg/l, C_2=2.5 mg/l and C_3=5 mg/l. The pH effect was studied over a range from 2 to 11, while the study of dye adsorption as a function of time was carried out over time intervals from 5 to 120 min. The adsorbent-adsorbate mixture was then separated using a high-speed centrifuge at 9000 rpm for 5 min. Absorbance was measured using a JENWAY UV/visible spectrometer at the wavelength corresponding to the dye's maximum absorbance (write the wavelength). The concentration of the dye was determined after plotting the calibration curve, so the adsorption capacity at time t was obtained by the Eq (A.5).

$$Q_t = \frac{(C_i - C_t)V}{m} \qquad \textbf{(Eq (A.5))}$$

Where Q_t is the quantity of dye adsorbed at time t in mg.g^{-1}, C_i is the initial concentration of dye in mg.L^{-1}, C_t is the concentration of dye at time t in mg.L^{-1}, V is the volume of the adsorbent-adsorbate mixture in L and m is the mass of material in g.

3. Results and discussion

3.1. Chemical analysis

The results of the chemical analysis of the three samples are presented in Table (B.1).

Table (B.1) Chemical composition of the three materials in percent by weight - GS: *Gelidium sesquipedale* - GSR: *Gelidium sesquipedale residue* - GRD: mixture of GSR and diatomaceous earth

Biomaterial	GS	GSR	GRD
Cellulose	13,31	20,29	10,87
Hemicellulose	3,98	6,12	5,03
Lignin	33,22	28,60	9,17
Agar	14.89	-	-
Substance mineral	00.70	17,24	67,57
Water content	07,63	07,73	02,26

The Table (B.1) shows that GRD is rich in mineral matter (67.57%), unlike GS (0.70%). This can be explained by the high quantity of silica in the GRD(Herzi, 2013; Vizinet and al., 1995). Whereas the mineral fraction of GSR (17.24%) can be explained by the effect of agar extraction on the organic fraction of red algae. Consequently, the dry organic matter content of GRD, GSR and GS are in the order of 30.17%, 75.03% and 91.67%, respectively.

The organic matter in the crystalline phase of the cell wall is mainly composed of cellulose, xylan and mannan(Garon-Lardière, 2004). Furthermore, the results in Table (B.1) show that GSR is rich in cellulose and hemicellulose compared to GS and GRD, with percentages of 20.29% and 6.12% respectively, giving it a higher cation exchange capacity, and consequently an affinity for positively charged micropollutants. GRD is low in lignin, with a percentage of 9.17%. On the other hand, GS and GSR are rich in lignin, with contents of 33.22% and 28.60% respectively. Lignin is amorphous and contains hydrophobic groups, which could confer greater permeability if these materials are incorporated into a soil mixture at appropriate proportions. This aspect has a definite impact on treatment processes such as filtration using biomaterials, as in the case of the multi soil layering system, where a soil mixture composed of, among other things, soil and sawdust is used(Mugani and al., 2024). In addition, *Gelidium sesquipedale* contains a significant amount of agar, representing 14.89%.

Compared with other plant species, the lignin content of GSR is lower than that of date palm (*Phoenix dactylifera)*(Kriker, 2005), while that of GS is comparable, and both are higher than that of sisal. The lignin content of GRD is comparable to that of sisal and lower than that of date palm. Also, the cellulose fraction of GSR, GS and GRD is lower than that of date palm fiber and sisal fiber(Asma, 2015).

The moisture content of plant fibers depends on relative humidity and other structural parameters(Garat, 2018). Indeed, the moisture content of GS (7.63%) is comparable to that of GSR (7.73%) and higher than that of GRD, which is a drier substance (2.26%).

3.2. Microstructural characterization

3.2.1. FTIR analysis

Fourier transform spectroscopy (FTIR) analysis of the three samples is shown in Fig (B.1).

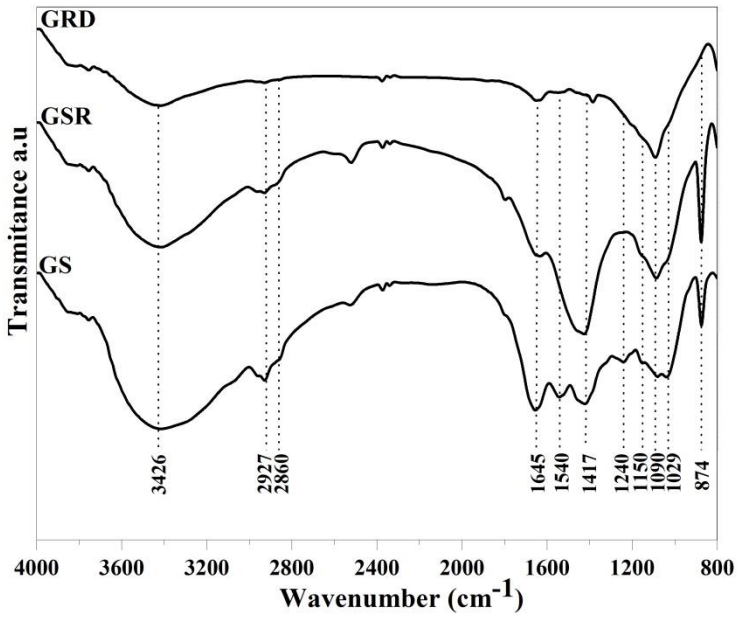


Fig (B.1) FTIR spectra of GS, GSR and GRD

The infrared spectra in Fig (B.1) shows the presence of a broad band located between 3000-3600 cm^{-1} corresponding to the stretching of the OH group present in cellulose, hemicellulose and lignin(Ajouguim and al., 2019; de Oliveira and al., 2019), as well as the Si-OH group(BENOUALI Djillali and al, 2016). The bands at 2927 cm^{-1} and 2860 cm^{-1} correspond to the elongation vibration of the CH and CH_2 groups present in cellulose, hemicellulose and lignin (Ajouguim and al., 2019; Boutorh, 2014; de Oliveira and al., 2019; Gomes-Dias and al., 2022; Méndez and al., 2019). In addition, the presence of proteins was identified by the presence of bands at 1645 cm^{-1} for amide I and 1540 cm^{-1} for amide II(de Oliveira and al., 2019). The peak at 1417 cm^{-1} represents the planar deformation of the CH group linked to the aromatic backbone(Rabemanolontsoa and Saka, 2013), in crystalline cellulose I, confirmed by the presence of the band at 1090 cm^{-1}(de Oliveira and al., 2019). The sulfate groups present in the agar structure are indicated by the peak at 1240 cm^{-1} corresponding to sulfate ester groups(Gómez-Ordóñez and Rupérez, 2011) and the band at 1150 cm^{-1} characterizing the vibration of the ester-sulfate bond(Guerrero and al., 2014). The band at 1029 cm^{-1} is attributed to the stretching of the CO and O-H groups in cellulose(Ajouguim and al., 2019; Gomes-Dias and al., 2022) and to the vibration of the siloxane group (Si-O -Si)(BENOUALI Djillali and al, 2016). Finally, the band located at 874 cm^{-1} corresponds to the stretching of the C-O-C group attributed to the β-glycosidic bonds present in cellulose(Ajouguim and al., 2019).

Comparing the peaks of the spectra, it can be seen that the intensity of the peaks at 1645 cm^{-1} and 1540 cm^{-1} indicating the presence of proteins, and those at 1240 cm^{-1} and 1150 cm^{-1} reflecting the presence of agar-agar, are lower for GSR than for GS. However, the intensities of peaks at 1427 cm^{-1}, 1090 cm^{-1} and 487 cm^{-1} representing cellulose are greater for GSR. This is due to the degradation of proteins during the agar-agar extraction process, and the consequent increase in the cellulose fraction. Similarly, there was a slight decrease in the intensity of peaks located at 3426 cm^{-1}, 2927 cm^{-1} and 2860 cm^{-1}, which can be explained by the degradation of lignin and hemicellulose. GRD peak intensities are lower than those of GS and GSR, with the exception of the peak at 1090 cm^{-1}, which has an intensity comparable to that of GS and GSR. This reflects the significant presence of the Si-O-Si bond in GRD.

3.2.2. X-ray diffraction (XRD) analysis

The X-ray diffraction analyses are shown in Fig (B.2).

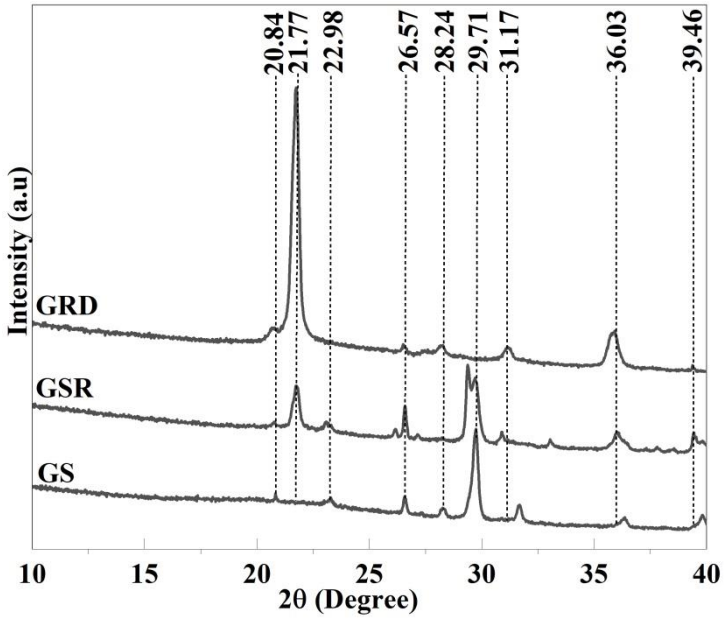


Fig (B.2) XRD spectra of GS, GSR and GRD - GS: *Gelidium sesquipedale* - GSR: *Gelidium sesquipedale* residue - GRD: mixture of GSR and diatomaceous earth

In order to assess the crystalline structure of GS, GSR and GRD, we carried out X-ray diffraction analyses, and the diffractograms obtained are presented in Fig (B.2). A peak located at 2θ=20.84° indicates the presence of amorphous agar(Martínez-Sanz and al., 2019), while peak located at 22.98° show the presence of crystalline planar cellulose I(de Oliveira and al., 2019). In addition, the peak located at 2θ=26.57° corresponds to the presence of nanocellulose(de Oliveira and al., 2019). Also, the peak at 2θ=29.71° also reflects the presence of cellulose(de Oliveira and al., 2019). The narrow peak located at 21.77° indicates the presence of mineral components naturally present in Gelidium algae, such as silica (SiO_2) and weddellite (CaC_2O_4-$2H_2O$)(Martínez-Sanz and al., 2019), also cristobalite for diatomaceous earth(Barbieri and al., 2020), the latter being the most intense peak. The two peaks at 28.24° and 31.17° are due to crystalline components such as minerals and salts ($CaCO_3$, $MgCO_3$)(Cebrián Lloret, 2024; Ferrera Lorenzo, 2012), the peak at 36.03° indicates the presence of calcite(Tahir Fazal1 and al., 2019) and cristobalite(Barbieri and al., 2020), while the peak at 39.46° reflects the presence of cellulose(Cebrián Lloret, 2024).

The crystallinity value estimated from XRD diagrams by OriginePro for raw *Gelidium sesquipedale* GS is 10.02%, comparable to that of *Gelidium sesquipedale* studied by Jean Paulo de Oliveira (10.9%)(de Oliveira and al., 2019) and lower than that of *Gelidium sesquipedale* studied by Marta Martínez-Sanz et al(Martínez-Sanz and al., 2019). GSR (12. 18%) has a higher crystallinity index than GS, which can be explained by the degradation of amorphous components such as lignin and hemicellulose after agar extraction, while GRD has a lower crystallinity (3.83%), This is in agreement with the results obtained by FTIR spectroscopy of the three samples and confirmed by the chemical composition studied previously, which shows an increase in cellulose content in GSR due to the degradation of lignin and hemicellulose in the GS structure, and a decrease in organic composition in GRD.

3.2.3. Scanning electron microscopy SEM/EDX.

Microscopic observation allows us to visualize the outer surfaces of all three materials. The results are shown in Fig (B.3).

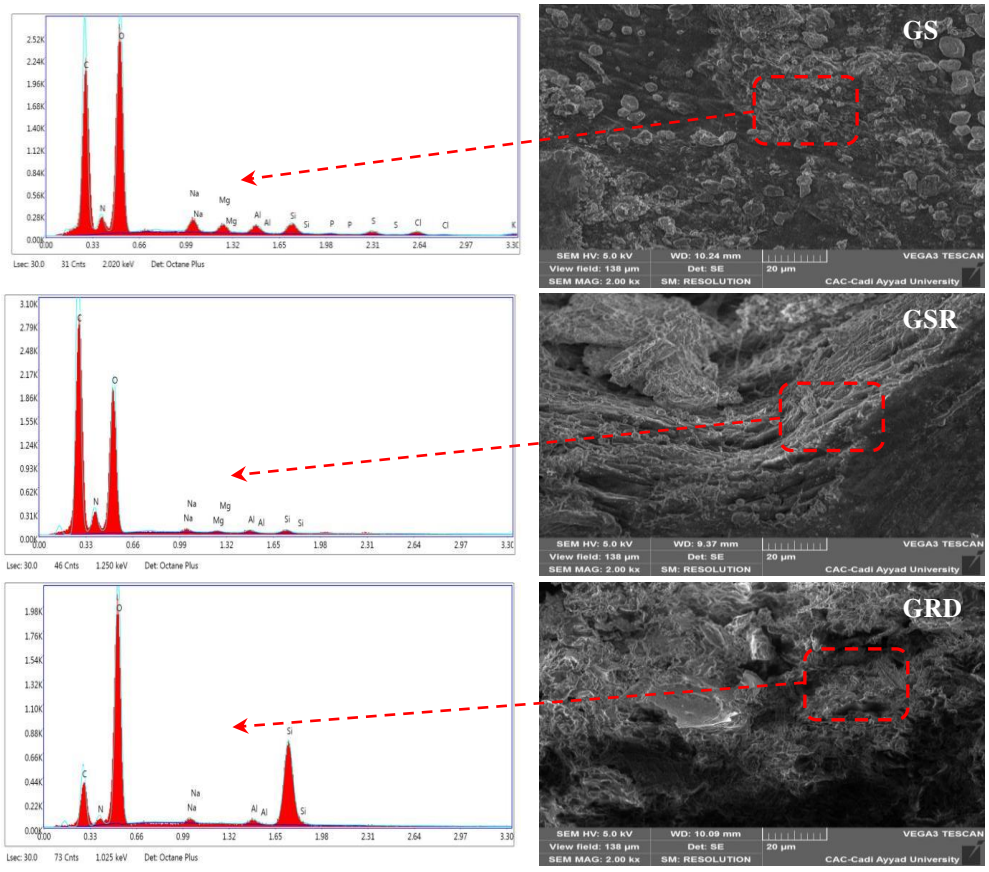


Fig (B.3) Structure of the outer surfaces of GS, GSR and GRD

Microscopic observation allows us to visualize the outer surfaces of the three materials. The results are illustrated in the figure below (Fig (B.3)). The analysis of these results showed a rough, highly irregular, porous structure over the majority of the GS outer surface. For GSR, the surface is marked by the presence of fibrous bundles glued together and spaced by voids, which can be explained by the previously highlighted cellulose fraction (20.29%) and the reduction of amorphous matter such as lignin and hemicellulose during the agar extraction process. Next, examination of the GRD's outer surface shows that it is not very rough, with heterogeneity in pore shape over most of the surface. Smooth, whitish crystalline structures corresponding to silica can also be observed.

Table (B.2) Mass percentages of chemical elements in GS, GSR and GRD

Chemical elements	C	N	O	Na	Mg	Al	Si	P	S	Cl
GS	32,91	5,25	39,60	2,92	1,91	2,67	4,97	0,71	3,70	5,37
GSR	47,57	9,86	37,84	0,86	0,51	1,29	2,07	-	-	-
GRD	12,70	2,68	42,06	0,95	1,56	-	40,04	-	-	-

The chemical composition of the surface of the three samples is shown in Table (B.2). The analysis of the samples studied revealed high levels of carbon (C) and oxygen (O) in GS and GSR (Table (B.2)), indicating the presence of organic matter. Microscopic examination also reveals the presence of cations such as (Na), (Mg), and (Al) on the external surface, visible in the peaks and in the Electron Beam Dispersion (EBD) microanalysis. Moreover, the presence of these cations could be a factor in reducing the adsorption potential, as they occupy the available sites(Alaa H. Hawari, 2005).

The examination of the outer surface of the three materials provides information on their behavior in contact with polluted water. It's clear that porous surfaces offer greater contact time between the materials and the pollutants in the water. Surfaces containing trace elements such as silica are favorable to cation exchange, with the GRD showing a large silica peak with a corresponding surface composition of 40.04%. These results encourage the evaluation of these three materials for the adsorptive treatment of polluted water.

3.2.4. Chemical analysis by X-ray fluorescence

The results of chemical analysis by X-ray fluorescence are shown in Table (B.3).

Table (B.3) Chemical analysis by X-ray fluorescence (composition in % by mass) - GS: *Gelidium sesquipedale* - GSR: *Gelidium sesquipedale* residue - GRD: The mixture of diatomaceous earth powder and *Gelidium sesquipedale* residue and D: Diatomaceous earth powder

Compound	SiO_2	Fe_2O_3	Al_2O_3	Na_2O	P_2O_5	TiO_2	CaO	K_2O	MgO	SO_3
GS	0,3689	0,0253	0,1643	0,9152	0,2382	0,0026	0,1716	0,987	0,5114	1,625
GSR	8,013	0,475	0,975	0,8941	2,055	0,1831	21,04	0,1451	2,904	2,02
GRD	72,23	1,844	3,332	2,928	1,7	0,4401	1,806	0,1551	0,6167	1,013
D	88,26	4,055	2,526	1,979	0,7795	0,6697	0,5612	0,2542	0,1837	0,1625
	MnO	BaO	Br	Cl	I	V_2O_5	Cr_2O_3	SrO	ZrO_2	NiO
	0,0017	0,0663	0,069	1,883	0,0429	0,0476	0,0096	0,0015	0,0104	0,0013
	0,026	-	0,336	0,4068	0,1374	0,0459	0,0111	0,1444	0,0186	0,0056
	0,0082	-	0,1164	0,0834	0,0662	-	0,0239	0,0121	-	0,0077
	0,0889	-	-	-	-	-		0,0195	-	0,0121
	CuO	ZnO	SnO_2	Co_3O_4	Nb_2O_5	Rb_2O	Ga_2O_3	Y_2O_3	As_2O_3	P.a.f
	0,0016	0,0034	0,0088	0,0069	0,0023	0,0038	0,0037	0,0016	0,0003	92,99
	0,0039	0,0121	-	-	0,0048	-	-	0,0014	-	60,21
	0,0106	0,0073	-	-	-	-	-	-	-	13,56
	-	0,0075	-	-	-	-	-	-	-	0,255

The XRF chemical analysis of the three samples shows that GRD is rich in silica (SiO_2) at 72.23%, compared with GSR and GS at 8.01% and 0.36% respectively (Table. (B.3)). we also analyzed diatomaceous earth alone (D), which is 88.26% silica. GSR is also rich in calcium (Ca) in the form of lime (CaO), with a composition of

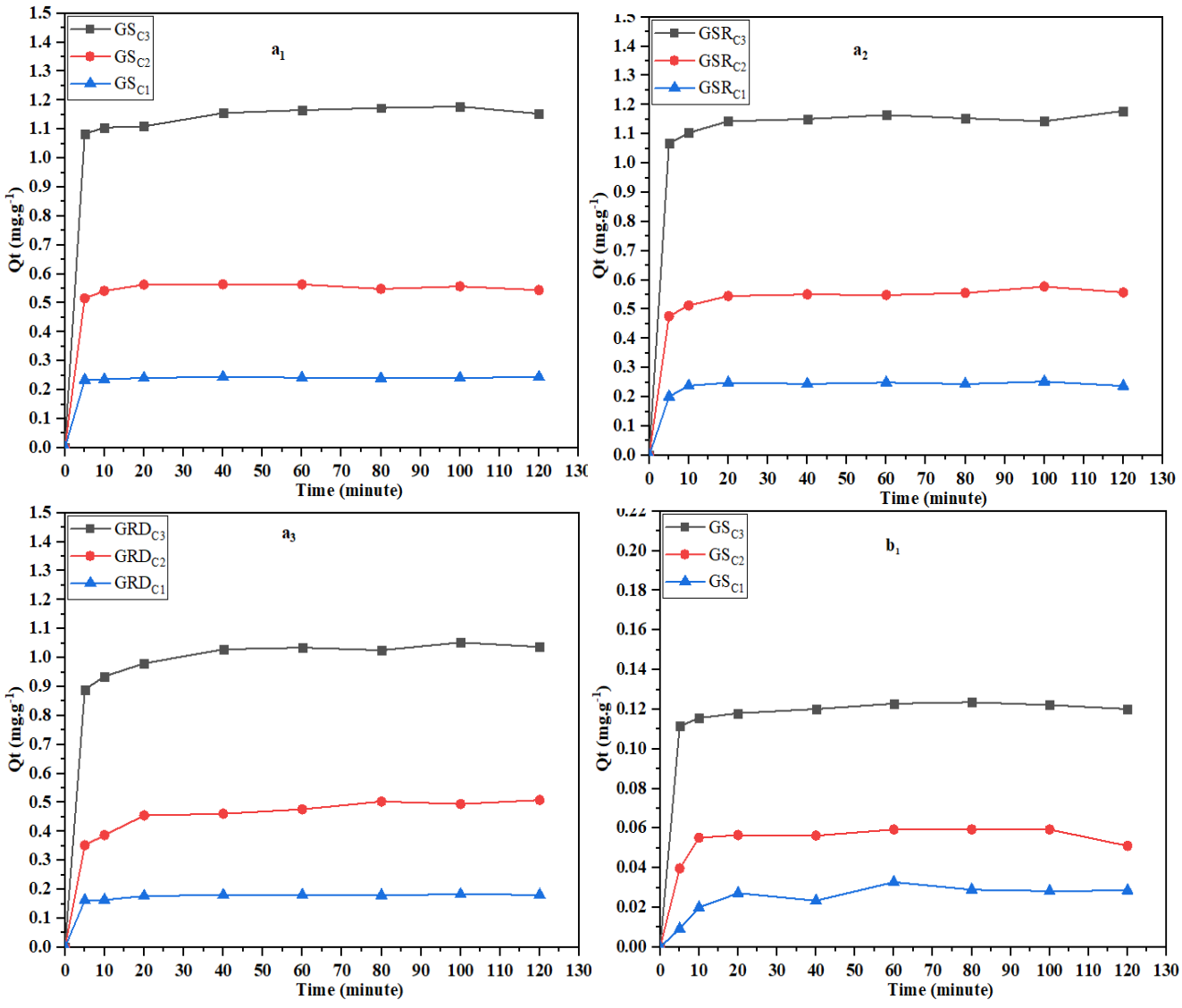
21.04%. The results also show the presence of other mineral salts in small quantities in the samples, namely iron (Fe_2O_3), aluminum (Al_2O_3) and phosphorus (P_2O_5), which do not exceed 4%. Other mineral elements (Na, Al, K, etc.) are present in very small quantities. In addition, GS and GSR are rich in carbon compared to GRD, with contents of 25.38% and 16.43% respectively. As a result, they are a good source of carbon for bacteria in the pollutant biodegradation process. Sawdust, for example, has been used in multilayer filters as a source of carbon for bacteria(Kuniaki Sato, 2010). The addition of sawdust to earth bricks for wastewater filtration has led to a 12% improvement in COD abatement(Xin Chen, 2010). In order to determine the involvement of the three materials studied in this process, sawdust was analyzed by X-ray fluorescence. It was found to have a carbon content of 27.17%, slightly higher than GS.

The analysis of loss on ignition indicated that the mass loss for GS is higher (92.99%) than that for GSR (60.21%), which may be due to the degradation of organic matter after agar extraction. Whereas the low value of mass loss obtained for GRD (13.56%) is related to the high fraction of mineral substance present in this sample. These results confirm the chemical, infrared spectroscopic, X-ray diffraction and X-ray fluorescence analyses, which showed that the GRD is rich in silica (SiO_2) and the GS and GSR in organic matter.

3.3. Adsorption of methylene blue (MB) and methyl orange (MO)

3.3.1. Effect of initial concentration and time

The evolution of the quantity of BM and OM dyes adsorbed on the three samples as a function of time and the effect of initial concentrations are shown in Fig (B.4).



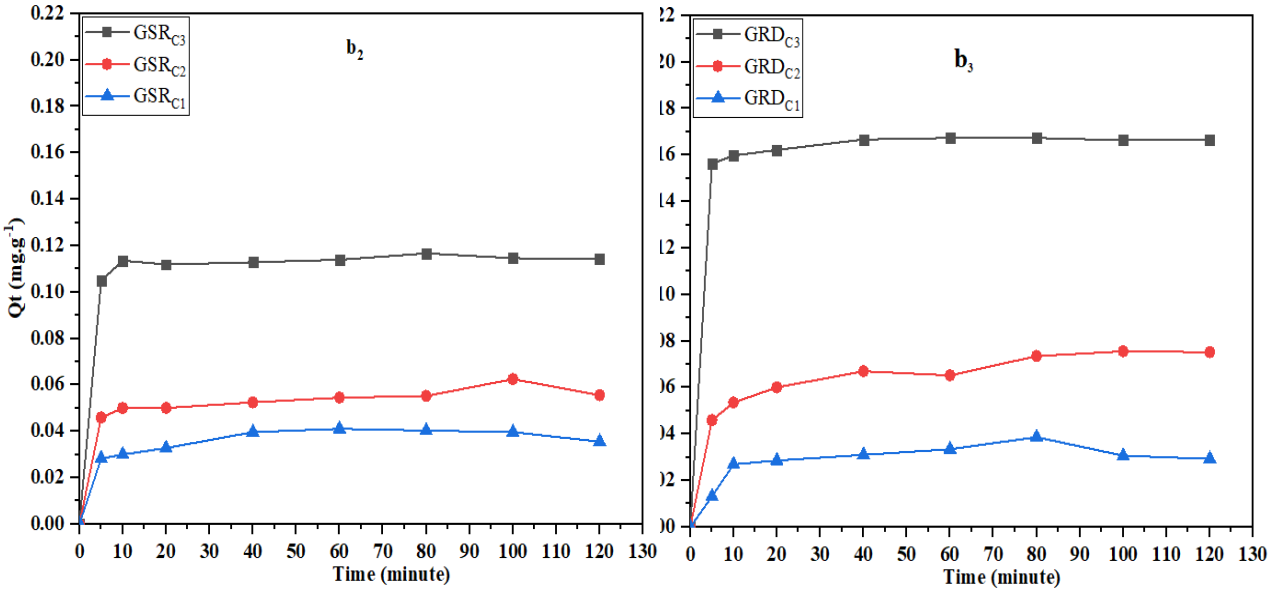


Fig (B.4) Adsorption of methylene blue (C_1 (4.12 mg.L^{-1}), C_2 (8.25 mg.L^{-1}) and C_3 (16.5 mg.L^{-1})) and methyl orange (C_1 (1.25 mg.L^{-1}), C_2 (2.5 mg.L^{-1}) and C_3 (5 mg.L^{-1})) on GS, GSR and GRD as a function of time – (a) Adsorption of BM – (b) Adsorption of OM

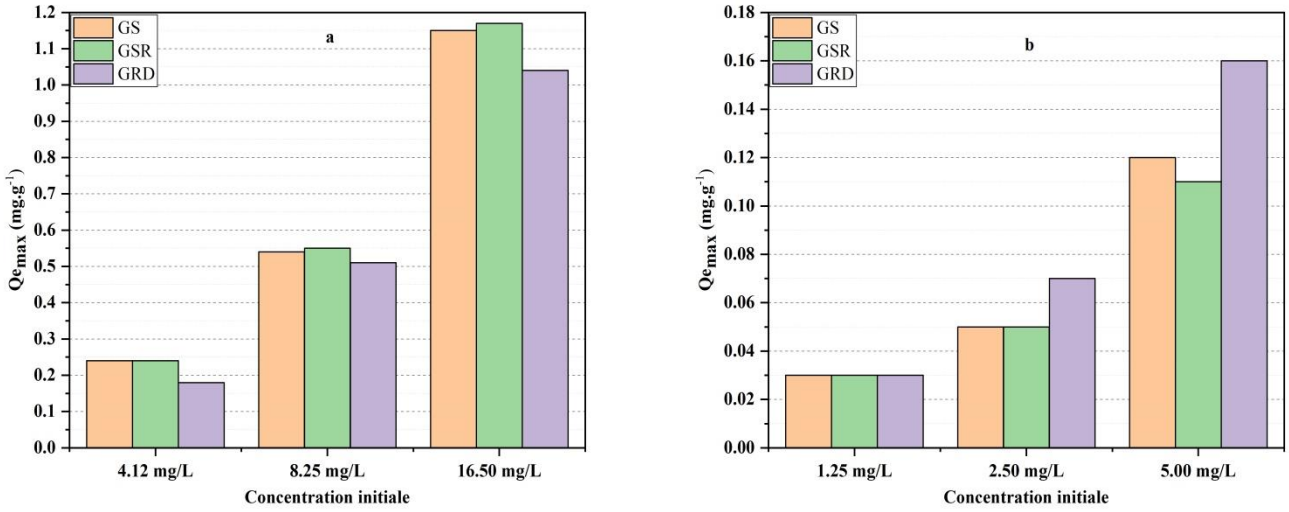


Fig (B.5) Maximum equilibrium quantity Qe_{max} as a function of initial concentration – (a) BM adsorption – (b) OM adsorption

The evolution of the quantity of MB and MO dyes adsorbed on the three samples as a function of time and the effect of initial concentrations are shown in the Fig (B.4). The analysis shows that the adsorption of two dyes as a function of time is characterized by two stages, a rapid stage in the first ten minutes, corresponding to diffusion of the dye onto the outer surface of the material, followed by a slow stage corresponding to intra-particle diffusion of the dye(F. Moughaoui*, 2017). Moreover, the amount of dye (BM or OM) at maximum equilibrium Qe_{max} increases as the initial concentration increases (Fig (B.5)). Comparing this amount, it can be seen that GSR and GS have a comparable maximum equilibrium adsorbed amount of methylene blue, which is greater than that of GRD. This is because an increase in concentration leads to an increase in the driving force of the concentration gradient, which in turn leads to an increase in dye diffusion within the material(Fayoud and al., 2015). All three materials can be said to have a greater affinity for MB.

3.3.2. Effect of pH

The effect of pH on the adsorption of BM and OM on the three materials was studied over a pH range from 2 to 11 as shown in Fig (B.6).

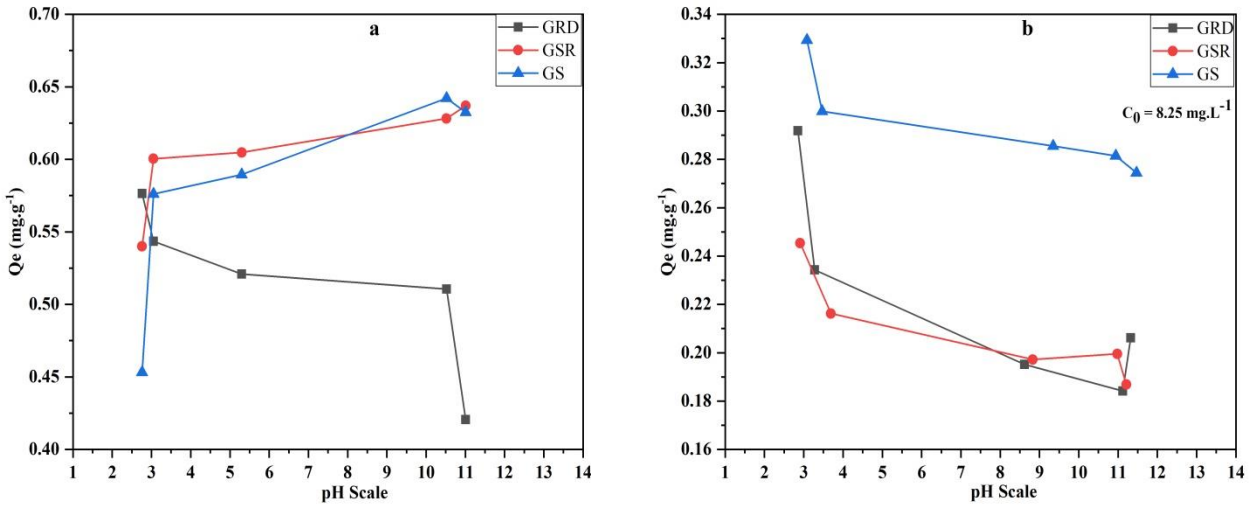


Fig (B.6) Influence of pH on adsorption - a) methylene blue (C_0=8.25 mg.L^{-1}) - b) methyl orange (C_0=5 mg.L^{-1}) on the three materials

The effect of pH on the adsorption of MB and MO on the three materials was studied over a pH range from 2 to 11 as shown in the Fig (B.6). The experiments were carried out by adjusting the pH of the mixture with a hydrochloric acid or sodium hydroxide solution. The results showed a significant increase in the amount of MB adsorbed on GS and GSR at pH=3. This can be explained by the fact that at low pH, the adsorbent surface (negatively charged site) would be surrounded by H^+ ions, reducing the interaction of methylene blue (Cation) ions with the adsorbent sites. On the other hand, at higher pH values, the H^+ concentration decreases, favoring effective interaction between dye ions and surface sites(F. Sakr, 2014).

The amount of MB adsorbed on GRD decreases around pH=3, and continues to fall significantly with increasing pH. Electrostatic repulsion and competition between H^+ ions and the cationic dye for adsorption sites are responsible for this decrease(Abdallah and al., 2016). The greatest quantities of MB adsorbed for GS and GSR are found at basic pH values between 10.5 and 11. GRD, on the other hand, seems to adsorb best at acidic pH.

MO adsorption shows that for all three algae, the amount adsorbed decreases with increasing pH. This decrease can be explained by the increase in OH^- ions present in the medium with increasing pH, resulting in competition with this anionic dye (MO) on adsorption sites(ABOUA and al., 2018). GRD showed a greater amount of MO adsorbed than GS and GSR.

3.3.3. Adsorption isotherm

Modeling of adsorption equilibria between the amount of dye in the liquid phase (Ce) and that adsorbed on the material (Qe) was treated by the Langmuir and Freundlich adsorption isotherms(Abdallah and al., 2016; Ainane, 2011; Fayoud and al., 2015).

- **Langmuir adsorption isotherm**

The Langmuir isotherm model (Fig (B.7)) assumes that the adsorbent active sites are identical and can complex a single solute molecule (monolayer adsorption), so there are no interactions between the adsorbed molecules, and the adsorbent material has a limited adsorption capacity (Q_{max})(Ainane, 2011; Fayoud and al., 2015). This model is represented by the formula presented in Eq (B.1).

$$\frac{1}{Q_e} = \frac{1}{C_e \; K_L \; Q_{max}} + \frac{1}{Q_{max}} \qquad \textbf{(Eq (B.1))}$$

C_e the equilibrium concentration ($mg.L^{-1}$) - Q_e the quantity adsorbed at equilibrium ($mg.g^{-1}$) - K_L is the equilibrium constant relative to the Langmuir model, and Q_{max} is the maximum quantity adsorbed ($mg.g^{-1}$).

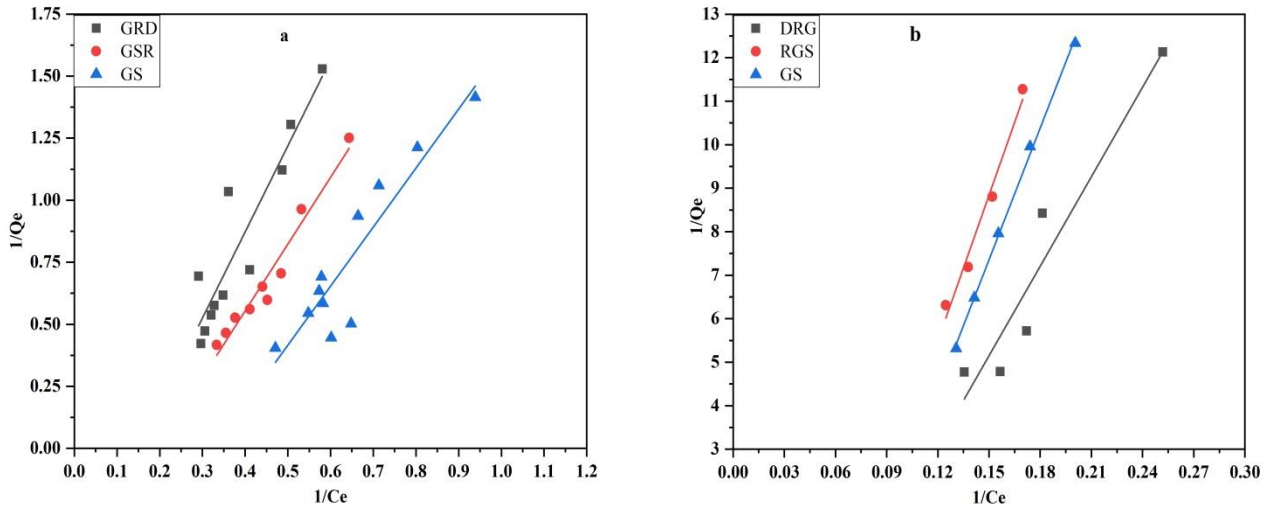


Fig (B.7) Langmuir isotherm for adsorption of - a) methylene blue - b) methyl orange on the three materials

- **Freundlich adsorption isotherm**

The Freundlich adsorption isotherm (Fig (B.8)) applies in the case of multilayer adsorption with the possibility of the presence of interactions between the adsorbed molecules, and is presented by the logarithmic equation in Eq (B.2).

$$LnQ_e = LnK_F + n*LnC_e \qquad \textbf{(Eq (B.2))}$$

K_F is the constant relative to the Freundlich model

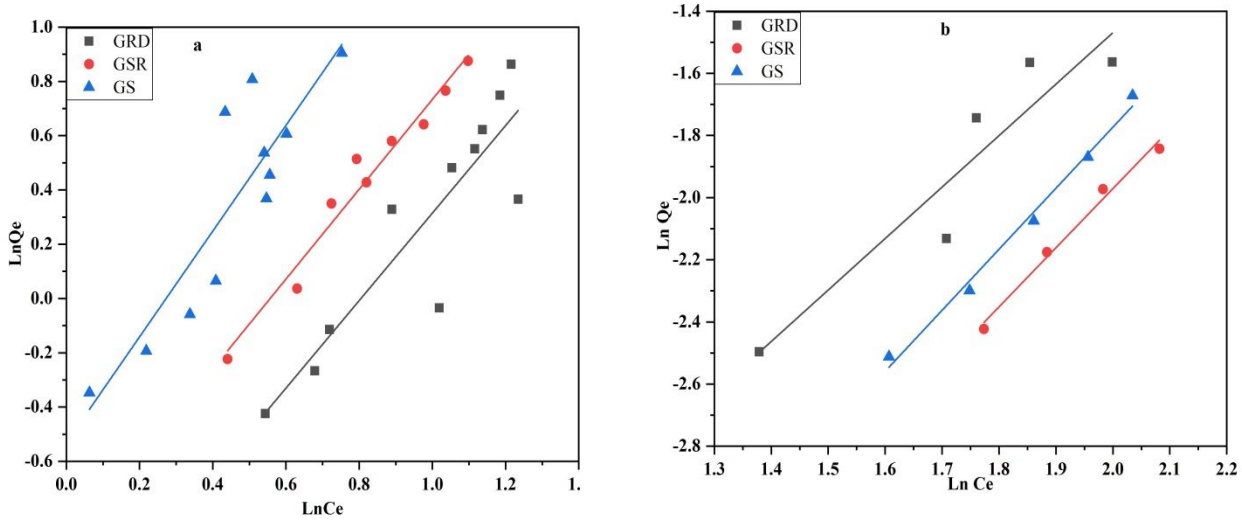


Fig (B.8) Freundlich isotherm for adsorption of - a) methylene blue - b) methyl orange on the three materials

Table (B.4) Adsorption parameters for methylene blue (MB) and methyl orange (MO) on the three materials

Adsorption isotherm		Langmuir			Freundlich		
Parameter		Q_{max} ($mg.g^{-1}$)	K_L	R^2	1/n	K_F	R^2
Methylene blue	GRD	-1,939	-0,149	0,8546	0.620	0.273	0.800
	GSR	-1,913	-0,194	0,9567	0.604	0.397	0.965
	GS	-1,292	-0,326	0,8493	0.513	0.587	0.782
Methyl orange	GRD	-0,194	-0,075	0,9189	0,604	0,008	0,8838
	GSR	-0,126	-0,071	0,9801	0,525	0,003	0,9874
	GS	-0,128	-0,077	0,9982	0,509	0,003	0,9907

The Table (B.4) revealed that the values representing the maximum Q_{max} quantities of both adsorbed dyes are negative, which has no physical significance(Aloui and Zertal, 2016). This negative value is probably due to the weight of the isotherm points corresponding to very low dye concentrations(Sakr and al., 2015). Furthermore, it was not possible to establish the K_L parameter using Q_{max}. As a result, the adsorption of the two dyes on the three materials cannot be described by the Langmuir model. Indeed, the Freundlich model assumes the formation of multilayers for both dyes. The intensity of adsorption and the relative distribution of energy sites for adsorption are indicated by the coefficient 1/n, which varies according to the nature of the strength of the adsorption process. Indeed, if 1/n is equal to 1, adsorption is linear; if it is greater than 1, adsorption is physical; if it is less than 1, adsorption is a favorable chemical process(Kifuani and al., 2018). The values of 1/n obtained in our situation are less than 1, suggesting that the adsorption of the two dyes on the three materials is favorable and corresponds to a chemical process.

3.3.4. Adsorption kinetic models

The thermodynamic equilibrium between the amount of dye in the liquid phase and the amount of dye bound to the solid kinetically comprises three stages; diffusion through the film surrounding the particles, diffusion into its pores and the adsorption/desorption reaction(Ainane, 2011; Fayoud and al., 2015). This equilibrium has been studied by three models: the pseudo-first-order kinetic model, the pseudo-second-order kinetic model and the intra-particle diffusion model.

- **Pseudo-first-order and pseudo-second-order kinetic models.**

The influence of time on dye retention on the three materials was studied using pseudo-first-order and pseudo-second-order kinetic models.

The pseudo-first-order kinetic model was modeled by the linear Eq (B.3)(Ainane, 2011; Fayoud and al., 2015). The results obtained by this model are illustrated in Fig (B.9).

$$ln\,(Q_e - Q_t) = -K_1 t + lnQ_e \quad \textbf{(Eq (B.3))}$$

K_1: rate constant for pseudo-first-order kinetics - Q_t: adsorption capacity at time t - Q_e: adsorption capacity at equilibrium.

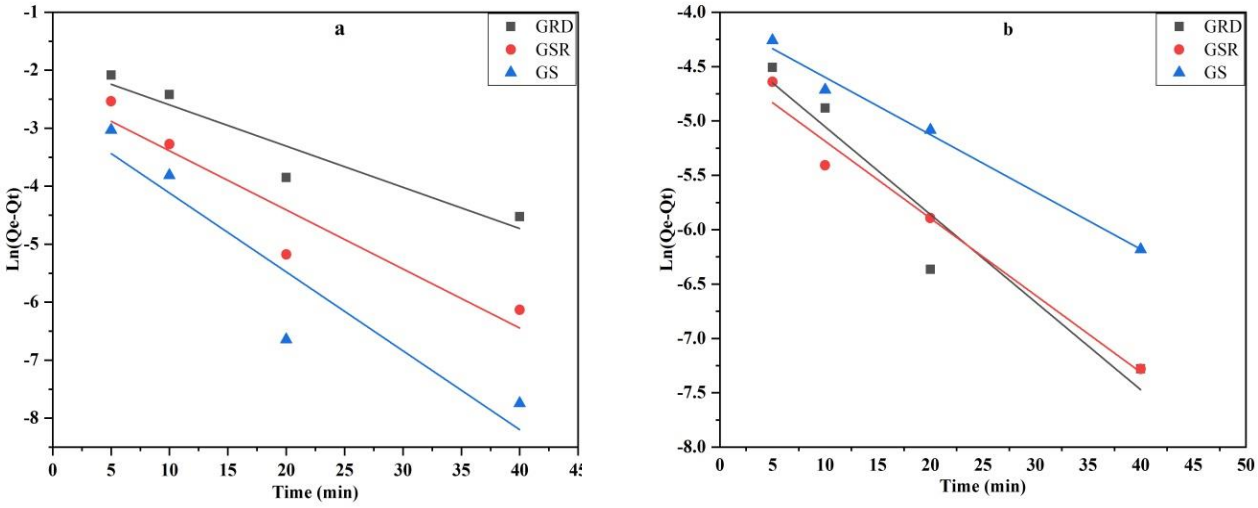


Fig (B.9) Pseudo-first-order kinetic model applied to the adsorption of - a) methylene blue - b) methyl orange on the three materials

The pseudo-second-order kinetic model has been modeled by the linear Eq (B.4)(Ainane, 2011; Fayoud and al., 2015). The results obtained are shown in Fig (B.10).

$$\frac{t}{Q_t} = \frac{t}{Q_e} + \frac{1}{K_2\, Q_e^2} \qquad \textbf{(Eq (B.4))}$$

K_2: rate constant for pseudo-second-order kinetics - Q_t: adsorption capacity at time t - Q_e: adsorption capacity at equilibrium.

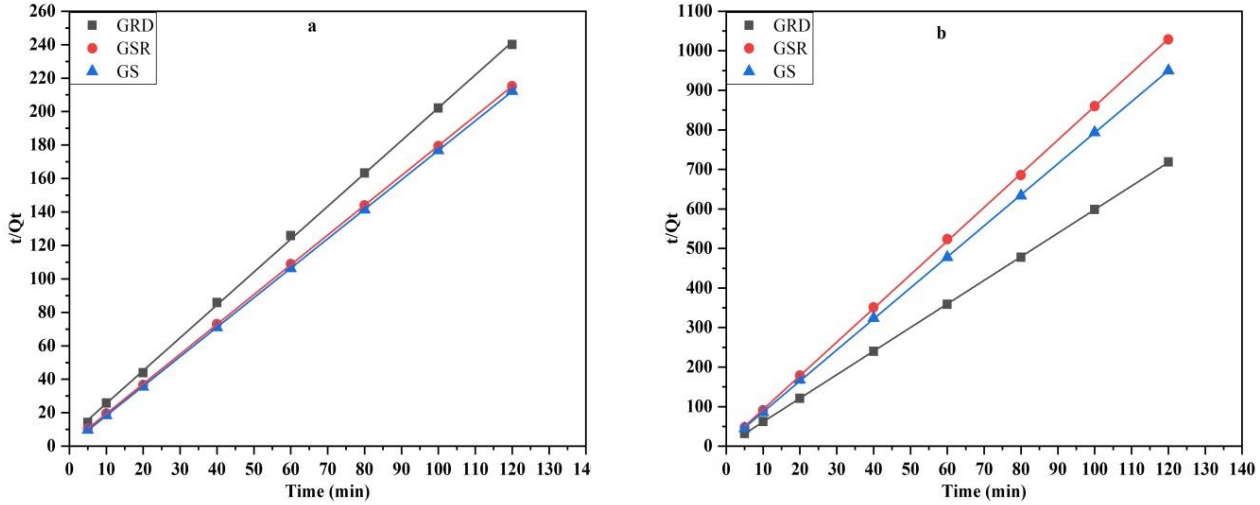


Fig (B.10) Pseudo-second-order kinetic model applied to the adsorption of - a) methylene blue - b) methyl orange on the three materials

Table (B.5) Kinetic parameters for methylene blue and methyl orange adsorption on DRG, RGS and GS

Kinetic parameter		MB			MO		
		C_0 = 8,25mg.L^{-1}			C_0 = 5 mg.L^{-1}		
		GRD	GSR	GS	GRD	GSR	GS
Pseudo-first-order	Qe_{the} (mg.g^{-1})	0,151	0.093	0.063	0.014	0.011	0.017
	K_1 (min^{-1})	0,071	0,101	0,136	0,080	0,070	0,052
	R^2	0,9024	0,9010	0,8793	0,932	0,976	0,989
Pseudo-second-order	Qe_{the} (mg.g^{-1})	0,509	0,561	0,567	0,167	0,117	0,127
	K_2(g.mg^{-1}.min^{-1})	0.66	1.969	5.144	19.916	9.745	8.052
	R^2	0,9997	0,9999	0,9999	0,9999	0,9999	0,9999
	Qe_{exp} (mg.g^{-1})	0,508	0,556	0,548	0,16	0,11	0,12

The results in the Table (B.5) show that the correlation coefficients for the pseudo-second-order kinetic model are higher, at around 0.99, than those obtained with the pseudo-first-order kinetic model, so that the quantities fixed at equilibrium (Qe_{The}) are comparable to the experimental values. As a result, adsorption of the two dyes on the three materials follows the pseudo-second-order kinetic model. The chemisorption is often described using this module. Many scientists have reported that the adsorption rates of dyes on bioadsorbents correspond to the assumptions of the pseudo-second-order model, which states that the molecules interact with the various surface functional groups of these adsorbents(Diop and al., 2022; Gueye, 2015), these results confirm the hypothesis that MB adsorption on biomaterials is mainly due to surface functional groups(Diop and al., 2022; Joseph, 2009).

- **Adsorption mechanism**

Intra-particle diffusion has been identified by the Webber-Morris relationship and is expressed by Eq (B.5).

$$Q_t = K_i * t^{0,5} + C \qquad \textbf{(Eq (B.5))}$$

K_i is the intraparticle diffusion velocity constant - C: is the y-intercept value, provides an indication of the boundary layer thickness.

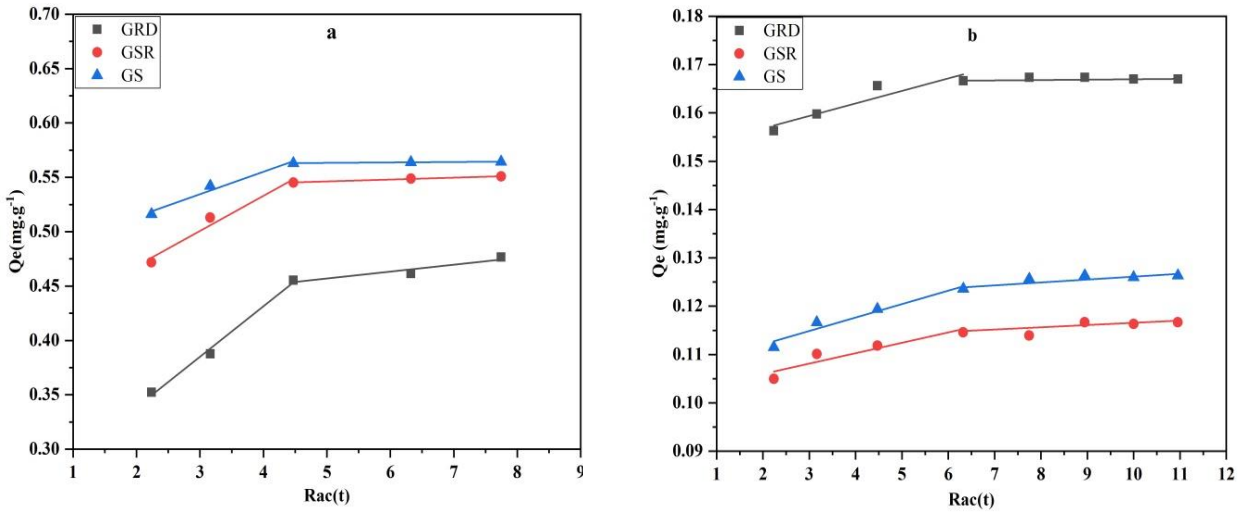


Fig (B.11) Intraparticle diffusion for adsorption of – a) methylene blue - b) methyl orange on the three materials

Table (B.6) Intra-particle diffusion parameters for methylene blue and methyl orange adsorption on the three materials

Kinetic parameter		MB			MO		
		C_0 = 8,25 mg.L^{-1}			C_0 = 5 mg.L^{-1}		
		GRD	GSR	GS	GRD	GSR	GS
Intra-particle diffusion	K_{i1} (mg.g^{-1}.min$^{-1/2}$)	0.0464	0.0322	0.0206	0,0026	0,0021	0,0028
	C_1	0.2457	0.4038	0.4725	0,1516	0,1017	0,1065
	R_1^2	0.9932	0.9712	0.9737	0,8770	0,8825	0,9493
	K_{i2} (mg.g^{-1}.min$^{-1/2}$)	0.0063	0.0017	0.0004	7,9838.10^{-5}	4,6360.10^{-4}	6,0206.10^{-4}
	C_2	0.4252	0.5375	0.5613	0,1661	0,1119	0,1201
	R_2^2	0.9019	0.9968	0.987	0,9618	0,8125	0,8160

As shown in Fig (B.11), the curves are distinguished by two distinct parts: the first corresponds to adsorption of the dye onto the material surface, while the second represents intra-particle diffusion of the dye onto the material pores. As expected, the diffusion rate constant Ki_1 is higher than that of the second stage Ki_2 (Table (B.6)). Firstly, the two dyes are fixed on the surface of all three materials rapidly, after saturation of the outer surface the dyes diffuse slowly between the pores of the materials. On the other hand, the fixation rates of methylene blue are higher than those of methyl orange on all three materials and for both stages. Compared with the other materials, GRD has the highest adsorption rate for methylene blue.

4. Conclusions

We analyzed three biomaterials using different techniques and methods: *Gelidium sesquipedale* algae, *Gelidium sesquipedale* algae residues and a mixture of diatomaceous earth and algae residues. A number of insights have been gained into the potential of these biomaterials for a variety of applications, including wastewater treatment.

The alga *Gelidium sesquipedale* undoubtedly offers interesting potential for applications in wastewater treatment. However, the excessive exploitation of this resource in recent years may lead us to think in terms of a circular economy, in favor of the use of residues, which have shown a potential comparable to that of the algae, with a methylene blue adsorption efficiency of 88%. In fact, they are richer in cellulose (GSR) and silica (GRD). SEM/EDX also revealed a surface favorable to adsorption and contact with pollutants. The study of methylene blue and methyl orange adsorption on the three biomaterials showed an affinity for methylene blue. In this sense, (GS) and (GSR) have greater potential than GRD and could be an alternative for the decontamination of industrial water containing dyes. Also, for the removal of cationic pollutants from domestic wastewater.

- **Competing interests**
  - The authors reports equipment or supplies was provided by Mohammed V University of Rabat, and Cadi Ayyad University of Marrakech..
  - The authors declare that they have no known competing financial interests or personal relationships that could have appeared to influence the work reported in this paper.
  - No funding was received to assist with the preparation of this manuscript.

- **Data availability**

The authors declare that the data supporting the findings of this study are available within the paper and its Supplementary Information files. Should any raw data files be needed in another format they are available from the corresponding author upon reasonable request.

References

Abdallah, M., Hijazi, A., Hamieh, M., Alameh, M., Toufaily, J., Rammal, H. J. J. o. M., & Science, E. (2016). Étude de l'adsorption du Bleu de Méthylène sur un biomatériau à base de l'eucalyptus selon la taille des particules Treatment of industrial wastewater using a natural and biodegradable adsorbent based on Eucalyptus. 7, 4036-4048.

ABOUA, K. N., SORO, D. B., DIARRA, M., DIBI, K., N'GUETTIA, K. R., & TRAORE, K. S. J. A. s. (2018). Étude de l'adsorption du colorant orange de méthyle sur charbons actifs en milieu aqueux: influence de la concentration de l'agent chimique d'activation. 14(6), 322-331.

Abraham, A., Afewerki, B., Tsegay, B., Ghebremedhin, H., Teklehaimanot, B., Reddy, K. S. J. I. J. o. M. B., & Research. (2018). Extraction of agar and alginate from marine seaweeds in red sea region. 3(2), 1-8.

Ainane, T. (2011). Valorisation de la biomasse algale du Maroc: Potentialités pharmacologiques et Applications environnementales, cas des algues brunes Cystoseira tamariscifolia et Bifurcaria bifurcata. Faculté des Sciences Ben M'sik Université Hassan II Casablanca,

Ajouguim, S., Abdelouahdi, K., Waqif, M., Stefanidou, M., & Saâdi, L. J. C. (2019). Modifications of Alfa fibers by alkali and hydrothermal treatment. 26, 1503-1516.

Alaa H. Hawari, C. N. M. (2005). Biosorption of lead(II), cadmium(II), copper(II) and nickel(II) by anaerobic granular biomass.

Aloui, A., & Zertal, A. (2016). Etude de l'élimination du paracétamol par le charbon actif en milieu aqueux.

Asma, S. (2015). Elaboration des composites cimentaires à base de fibres végétales locales (le diss): caractérisation, durabilité et application au cas de la maçonnerie. Université Badji Mokhtar,

Asnaoui, H., Laaziri, A., & Khalis, M. J. M. J. o. C. (2017). Biosorption of chromium (Cr) onto algae (Ulva. lactuca): application of isotherm and kinetic models. 5(1), J. Chem. 5 N° 1 (2017) 2186-2195.

Barbieri, P. G., Somigliana, A., & Carradori, G. J. L. M. d. L. (2020). Silicosi severa da terre di diatomee nella produzione di alginato ad uso odontoiatrico: uno studio necroscopico. 111(3), 222.

Bengueddour, Y., El Hani, S., El Ibaoui, H., El Ayadi, R., Brhadda, N. J. N., & Technology. (2014). Etude de l'activité anti oxydante de Gelidium Sesquipedale par chromatographie liquide haute performance. 10, 29-33.

Benhissoune, S. (2002). Contribution à l'étude de la flore des macroalgues marines du Maroc (Méditerranée et Atlantique). Thèse Doctorat, Université Mohammed V Rabat,

BENOUALI Djillali, BELKANDOUCI Mohamed Mustapha, KHERICI Samira, O. UTILISATION DE LA DIATOMITE POUR L'ETALONNAGE D'UN CAPTEUR INFRAROUGE DE TURBIDITE DE L'EAU.

Bentahar, Y. (2016). Caractérisation physico-chimique des argiles marocaines: application à l'adsorption de l'arsenic et des colorants cationiques en solution aqueuse. COMUE Université Côte d'Azur (2015-2019); Université Abdelmalek Essaâdi …,

Boutorh, J. (2014). Impact des conditions nutritionnelles sur la dissolution de la silice biogénique des diatomées à travers l'étude de la variabilité de la structure biphasique du frustule. Université de Bretagne occidentale-Brest,

Cebrián Lloret, V. (2024). Valorization of marine biomass for the development of biopolymeric materials and additives with functional properties. Universitat Politècnica de València,

de Oliveira, J. P., Bruni, G. P., Fabra, M. J., da Rosa Zavareze, E., López-Rubio, A., & Martínez-Sanz, M. J. F. H. (2019). Development of food packaging bioactive aerogels through the valorization of Gelidium sesquipedale seaweed. 89, 337-350.

Dietrich, É. (2008). Synthèse et études physico-chimiques de verres bioactifs denses et poreux. Applications en tant que biomatériaux en sites osseux. Université Rennes 1,

Diop, A., Faye, M., Diedhiou, D., Diop, P. L. D., & Diop, C. M. J. A. S. (2022). Valorisation des coques de graines de neem, Azadirachta indica A. Juss, comme bioadsorbant: Application à l'élimination d'un colorant (bleu de méthylène). 20(6), 100-120.

Do Thi, V. V. D. T. (2011). Matériaux composites à fibres naturelles/polymère biodégradables ou non. Université de Grenoble; Université des Sciences Naturelles d'Ho Chi Minh Ville,
Elbariji, S., Elamine, M., Eljazouli, H., Kabli, H., Lacherai, A., & Albourine, A. J. C. R. C. (2006). Traitement et valorisation des sous-produits du bois. Application à l'élimination des colorants industriels. 9(10), 1314-1321.
F. Moughaoui*, M. B., A. Bennamara, A. Abourriche, Z. Anbaoui. (2017). Study of Adsorption Isotherms and Kinetic Models of Methylene Blue Adsorption on Moroccan Bagasse Waste.
F. Sakr, A. S., M. Elouardi, M. Tamimi, A. Assabbane. (2014). Étude de l'adsorption du Bleu de Méthylène sur un biomatériau à base de Cactus (Adsorption study of Methylene Blue on biomaterial using cactus).
Fayoud, N., Younssi, S. A., Tahiri, S., & Albizane, A. J. J. M. E. S. (2015). Etude cinétique et thermodynamique de l'adsorption de bleu de méthylène sur les cendres de bois (Kinetic and thermodynamic study of the adsorption of methylene blue on wood ashes). 6(11), 3295-3306.
Ferrera Lorenzo, N. (2012). Aprovechamiento integral del residuo sólido de la obtención de Agar-Agar y su aplicación en el campo de la Energía y el Medio Ambiente.
Gaël, R. (2005). Extraction, Détermination Structurale et Valorisation Chimique de Phycocolloïdes d'Algues Rouges. Université de Limoges,
Garat, W. (2018). Contribution à l'analyse dimensionnelle et mécanique des fibres végétales en environnement humide contrôlé. IMT-MINES ALES-IMT-Mines Alès Ecole Mines-Télécom,
Garon-Lardière, S. (2004). Etude structurale des polysaccharides pariétaux de l'algue rouge Asparagopsis armata (Bonnemaisoniales). Université de Bretagne Occidentale,
Givernaud, T., Sqali, N., Barbaroux, O., Orbi, A., Semmaoui, Y., Rezzoum, N. E., . . . Kaas, R. J. P. (2005). Mapping and biomass estimation for a harvested population of Gelidium sesquipedale (Rhodophyta, Gelidiales) along the Atlantic coast of Morocco. 44(1), 66-71.
Gomes-Dias, J. S., Pereira, S. G., Teixeira, J. A., & Rocha, C. M. J. F. H. (2022). Hydrothermal treatments–A quick and efficient alternative for agar extraction from Gelidium sesquipedale. 132, 107898.
Gómez-Ordóñez, E., & Rupérez, P. J. F. h. (2011). FTIR-ATR spectroscopy as a tool for polysaccharide identification in edible brown and red seaweeds. 25(6), 1514-1520.
Guerrero, P., Etxabide, A., Leceta, I., Peñalba, M., & De la Caba, K. J. C. p. (2014). Extraction of agar from Gelidium sesquipedale (Rodhopyta) and surface characterization of agar based films. 99, 491-498.
Gueye, M. (2015). Développement de charbon actif a partir de biomasses lignocellulosiques pour des applications dans le traitement de l'eau. Fondation 2iE,
Herzi, F. (2013). Caractérisation chimique des exsudats du dinoflagellé marin toxique Alexandrium catenella et de la diatomée marine Skeletonema costatum et étude de la réponse protéomique d'Alexandrium catenella en conditions de stress métalliques. Université de Toulon; Faculté des sciences de Bizerte (Tunisie),
Iwuozor, K. O., Ighalo, J. O., Emenike, E. C., Ogunfowora, L. A., Igwegbe, C. A. J. C. R. i. G., & Chemistry, S. (2021). Adsorption of methyl orange: A review on adsorbent performance. 4, 100179.
Joseph, O. (2009). Etude du potentiel d'utilisation de résidus agricoles haïtiens pour le traitement par biosorption d'effluents pollués. INSA LYON,
Kifuani, K. M., Mayeko, A. K. K., Vesituluta, P. N., Lopaka, B. I., Bakambo, G. E., Mavinga, B. M., . . . Sciences, C. (2018). Adsorption d'un colorant basique, Bleu de Méthylène, en solution aqueuse, sur un bioadsorbant issu de déchets agricoles de Cucumeropsis mannii Naudin. 12(1), 558-575.
Kone, M., Bonou, L., Koulidiati, J., Joly, P., Sodre, S., & Bouvet, Y. J. R. d. S. d. l. E. (2012). Traitement d'eaux usées urbaines par infiltration-percolation sur sable et sur substrat de coco après un bassin anaérobie de lagune sous climat tropical. 25(2), 139-151.
Kriker, A. (2005). Caractérisation des fibres de palmier dattier et propriétés des bétons et mortiers renforcés par ces fibres en climat chaud et sec. Alger, Ecole Nationale Polytechnique,
Kuniaki Sato, T. M. T. W. (2010). Characterization of Treatment Processes and Mechanisms of COD, Phosphorus and Nitroge Removal in a Multi-Soil-Layering System.
Lavoie, I., & Saulnier-Talbot, É. J. V., la revue de l'Association des biologistes du Québec. (2016). Les diatomées: petits chefs-d'oeuvre de la nature et microtechnologie 100% naturelle au service du biosuivi des écosystèmes aquatiques. 36(1), 10-12.
Martínez-Sanz, M., Gómez-Mascaraque, L. G., Ballester, A. R., Martínez-Abad, A., Brodkorb, A., & López-Rubio, A. J. A. R. (2019). Production of unpurified agar-based extracts from red seaweed Gelidium sesquipedale by means of simplified extraction protocols. 38, 101420.
Méndez, A., Gascó, G., Ruiz, B., & Fuente, E. J. B. t. (2019). Hydrochars from industrial macroalgae "Gelidium Sesquipedale" biomass wastes. 275, 386-393.
Mouhoubi, S., Bourahli, M., Osmani, H., & Abdeslam, S. J. J. o. N. F. (2017). Effect of alkali treatment on alfa fibers behavior. 14(2), 239-249.
Mugani, R., El Khalloufi, F., Aba, R. P., Haida, M., Essadki, Y., Zerrifi, S. E. A., . . . Campos, A. J. J. o. C. P. (2024). Innovative approaches for Microcystin removal: Bacterioplankton biodegradation and multi-soil-layering system performance assessment. 452, 142187.

Nagai, T., & Yukimoto, T. J. F. c. (2003). Preparation and functional properties of beverages made from sea algae. 81(3), 327-332.
Ouensanga, A. J. W., & science, f. (1989). Variation of fiber composition in sugar cane stalks. 105-111.
Qlihaa, A., Dhimni, S., Melrhaka, F., Hajjaji, N., & Srhiri, A. J. J. M. E. S. (2016). Caractérisation physico-chimique d'une argile Marocaine [Physico-chemical characterization of a morrocan clay]. 7(5), 1741-1750.
Rabemanolontsoa, H., & Saka, S. J. R. a. (2013). Comparative study on chemical composition of various biomass species. 3(12), 3946-3956.
Rout, A. K., Kar, J., Jesthi, D. K., & Sutar, A. K. J. B. (2016). Effect of surface treatment on the physical, chemical, and mechanical properties of palm tree leaf stalk fibers. 11(2), 4432-4445.
Sakr, F., Sennaoui, A., Elouardi, M., Tamimi, M., Assabbane, A. J. J. o. m., & Science, E. (2015). Étude de l'adsorption du Bleu de Méthylène sur un biomatériau à base de Cactus (Adsorption study of Methylene Blue on biomaterial using cactus). 6(2), 397-406.
Straub, F., Derleth-Sartori, P., & Lods-Crozet, B. J. B. d. l. S. v. d. S. n. (2014). Les diatomées (algues silicatées), indicatrices de la qualité des cours d'eau vaudois: synthèse 2005 à 2013. 94(1), 73-106.
Tahir Fazal1, , A. F., , A. M., , A. H., , F. J., , A. A. D., . . . Rehman1, F. (2019). Macroalgae and coal-based biochar as a sustainable bioresource reuse for treatment of textile wastewater.
Vizinet, J., De Reviers, B. J. V. e. M. L., & Environment. (1995). Les utilisations des diatomées. 301-314.
Wang, N., Ding, E., & Cheng, R. J. P. (2007). Thermal degradation behaviors of spherical cellulose nanocrystals with sulfate groups. 48(12), 3486-3493.
Xin Chen, K. S., Toshiyuki Wakatsuki & Tsugiyuki Masunaga. (2010). Effect of structural difference on wastewater treatment efficiency in multi-soil-layering systems: Relationship between soil mixture block size and removal efficiency of selected contaminants.
高橋裕一, & 日本水産学会誌, 片. J. (1987). Seasonal variation of the hemagglutinating activities in the red alga Gracilaria verrucosa. 53(12), 2133-2137.

Supplementary Files

This is a list of supplementary files associated with this preprint. Click to download.

- AnalysechimiquedeFluorescenceX.pdf
- EDXOfGRD.pdf
- EDXofGelidiumsesquipedaleresidues.pdf
- EDXofGelidiumsesquipedale.pdf
- FTIRspectraofGSGSRandGRD.pdf
- Freundlichisothermforadsorptionofmethylorange.pdf
- Freundlichisothermforadsorptionofmethyleneblue.pdf
- InfluenceofpHonadsorptionmethylorange.pdf
- InfluenceofpHonadsorptionmethyleneblue.pdf
- Intraparticlediffusionforadsorptionofmethylorange.pdf
- Intraparticlediffusionforadsorptionofmethyleneblue.pdf
- Langmuirisothermforadsorptionofmethylorange.pdf
- Langmuirisothermforadsorptionofmethyleneblue.pdf
- XRDspectraofGSGSRandGRD.pdf